CHANGES OF POLARIMETRIC SCATTERING CHARACTERISTICS OF ALOS PALSAR CAUSED BY VOLCANIC ASH FALL DETECTED BY THE UNSUPERVISED WISHART CLASSIFIER

Hiroshi OHKURA

Professor, Department of Global Environment Studies, Hiroshima Institute of Technology,

2-1-1 Miyake, Saeki-ku, Hiroshima, 731-5193, Japan; Tel: +81-82-921-5462;
E-mail: h.ohkura.x3@it-hiroshima.ac.jp

KEY WORDS: SAR, Polarimetry, Unsupervised classification, Volcanic ash

Abstract: POLSAR images of ALOS PALSAR of Shinmoedake volcano in Kyushu, Japan were analyzed. Eruptions of the volcano on 26th and 27th January, 2011 caused ash depth of more than 10 cm in 12 km^2 and 1 m in 2 km^2. Two images before and after the eruption were classified by the unsupervised classifier with the Wishart distance. And optimum total numbers of classified categories of the images are 11 and 17, respectively. From a view point of the four-component scattering model, the 11 categories can be coupled with the similar categories of the image after the eruption. Because remaining 6 categories changed the normalized total power and the ratio of surface scattering power to the total power, they are different from the 11 categories. Moreover, the ratio of double-bounce scattering power increases in one of the 6 categories

INTRODUCTION

Shinmoedake is a volcano in Kyushu, Japan (Figure 1), and a part of the Mount Kirishima cluster of volcanos. The 2011 eruptions of Shinmoedake began with infrasonic waves on 19 January. From 26 to 27 January, they became full-blown magmatic explosions with quasi-Plinian eruptions which is marked by ejection of the large amount of pumices and very powerful continuous gas blast eruptions.

Then, lava began to spurt into the volcanic mouth about 28 January. After the spurt ceased on 1 February, Vulcanian eruptions, which eject cinders and ashes explosively, repeated sporadically. After a tranquil condition continued from April, small scale activities, which spewed smoke from a crater to 200m-1000m, continued from the end of June. The volcanic earthquakes continued, although the diastrophism which showed supply of magma stopped in January 2012.

The eruptions from 26 to 27 January were the largest eruption of Shinmoedake since 1959. These two days' eruptions caused ash depth of more than 10 cm in 12 km^2 and 1 m in 2 km^2 (JMA, 2011). Full polarimetric SAR (POLSAR) images over Shimmoedake were acquired by ALOS before and after the two days' eruptions.

Because POLSAR data has much more information than the single polarimetric one, excellent methods for the POLSAR data to classify terrain and land use have been proposed (Lee, 1999, Lee, 2004, Xu, 2005, Cao, 2007). This paper reports analyzed results of the images by the unsupervised classifier. And changes of polarimetric scattering characteristics caused by volcanic ash-fall are discussed by examining the analyzed results from a viewpoint of the four-component scattering model.

Figure 1: The position of Shinmoedake

UNSUPERVISED CLASSIFIER FOR POLSAR

Lee et al. proposed the k-means method with the Wishart distance as an unsupervised classifier (Lee, 1999). This classifier is useful when supplemental information of the analyzing area is inadequate and in case of emergency. However it is difficult to fix the total number of classes or clusters for each image data because an optimum number cannot be found out a priori. The k-means method was developed to the ISODATA method and the robust method of defining the optimal total of a class was proposed (Ohkura, 2011).

The Wishart distance d defines distance between coherency matrices T of pixels of the POLSAR image data. The distance d between an ensemble $\langle T \rangle$ of the coherence matrix of n pixels and the matrix Vm which is a cluster mean of the mth class is expressed by the following equation (Lee 1999).

$$d\left(\langle T\rangle, V_m\right) = \ln\left|V_m\right| + \mathrm{Trace}\left(V_m^{-1}\langle T\rangle\right) \qquad (1)$$

Since the ISODATA method is based on an iteration algorithm, a converged result is not necessarily the best one which represents characteristics of the image data optimally. To search the optimum result, we evaluate the converged results and fix an optimum number of classes. A criterion for the evaluation is whether two different initial clusters of the same total number of classes converge on a same result.

The two different initial classes are made up as followings.
1) By using the same method of Lee et al. introduced (Lee, 1999), we divide the three dimensional space to N subspaces which is defined by the three axes of "the entropy", "the average of the alpha angle" and "the total power". Each pixel of the image is segmented into the classes according to the subspace which the pixel belongs to (Figure 2).
2) After extracting some number of pixels from the whole image by random sampling, we put them in the N classes using the hierarchical clustering based on the Ward method (Figure 3).

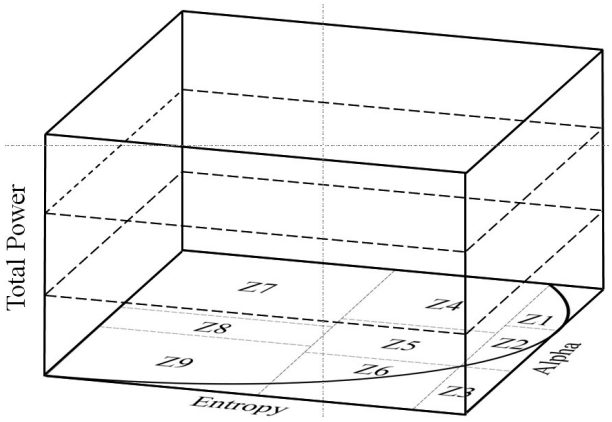

Figure 2: Initial clusters by domain segmentation of the H-α plane (N=28).

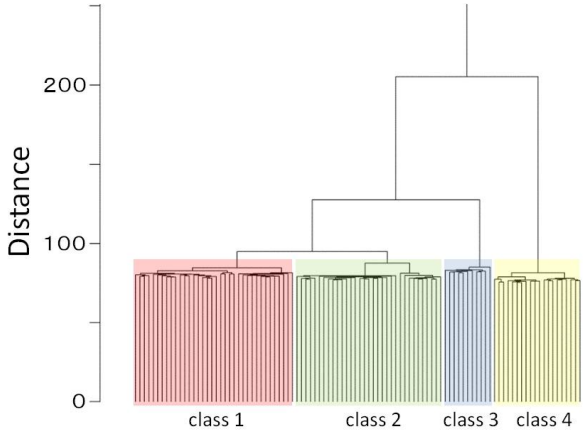

Figure 3: Initial clusters by the hierarchical clustering based on the Ward method (N=4).

We vary the total number N of classes of each initial set simultaneously, and the optimum number Nc is the N which makes a concordance rate of converged results maximum. The concordance rate C is defined by the following equation.

$$C = \frac{1}{N_p}\sum_{i=1}^{N}\max_{j=1,N}\left(M_i \cap S_j\right) \qquad (2)$$

where Np is the total number of pixels, subscripts i and j represent the i th class and the j th class respectively, and M and S are two sets of classified results corresponding to the two initial classes respectively.

In addition, to keep the total numbers of classes of M and S at same number, following two points are modified from the general IODATA method.
1) "Merging of classes" and "splitting of a class" are executed at every iteration.
2) "Removal of minimum clusters and isolated members" is not executed.
The modification 2) is for not missing changes of a very small domain at the time of the time series analysis.

UNSUPERVISED CLASSIFICATION OF POL SAR IMAGES OF ALOS OVER SHINMOEDAKE

The ALOS PALSAR PLR images of the volcano, which were acquired before and after the eruptions on 10 June 2009 and 16 March 2011 respectively, were analyzed. The study area is a rectangle of about 30 km by 30 km where Shinmoedake is in the center. Figure 4 is the original image of the study area on 10 June 2009.

Figure 5 shows variation of the concordance rate C versus the class number N of the image before the eruption. When N is 11, C becomes the maximum value of 0.99, and as N increases more, C trends toward a decrease. This shows that the optimum total number of classes Nc is 11. Figure 6 is the classified result of the optimum total number.

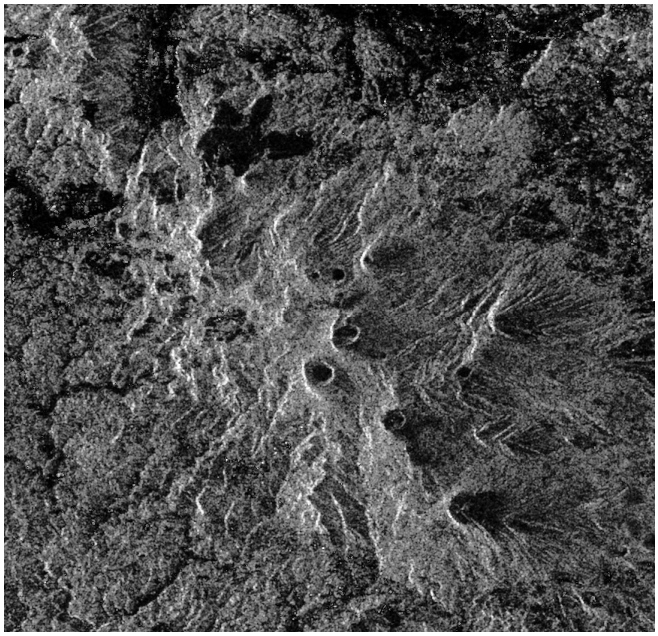

Figure 4: The original SAR image of Shinmoedake acquired before the eruption on 10 June 2009..

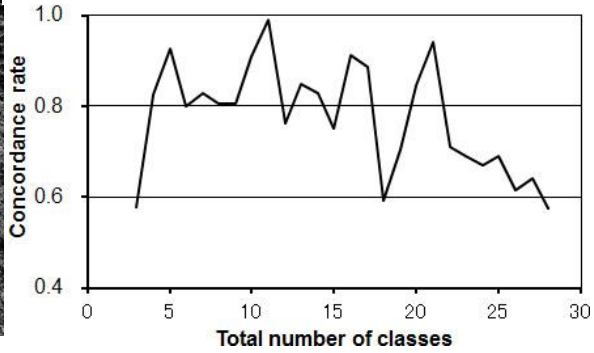

Figure 5: Concordance rate versus the total number of classes of the image before the eruption.

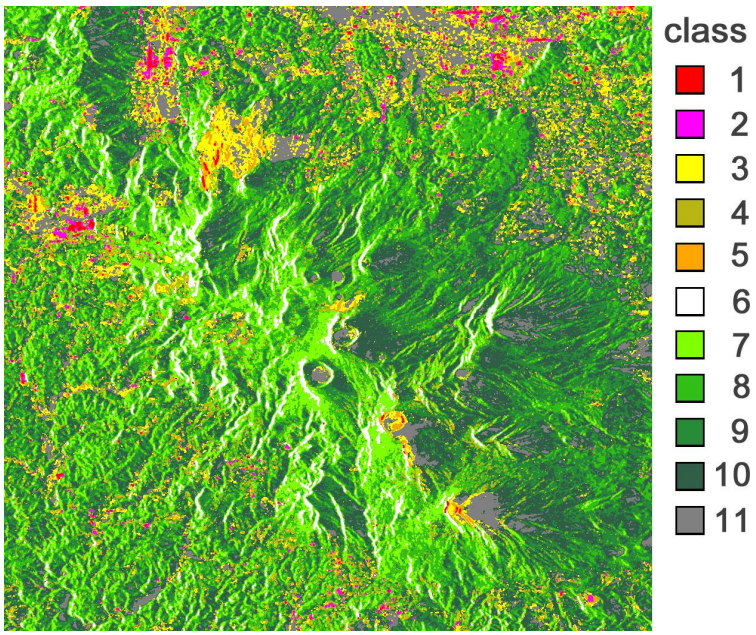

Figure 6: The classified result of the optimum total class number 11 of the image before the eruption.

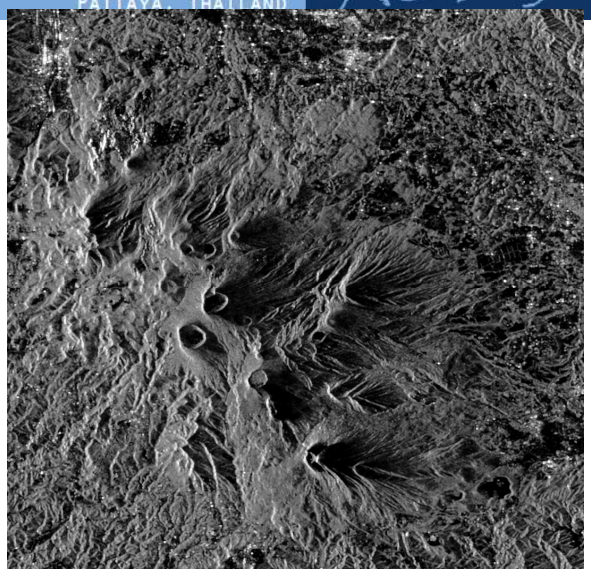

Figure 7: The original SAR image acquired after the eruption on 16 March 2011..

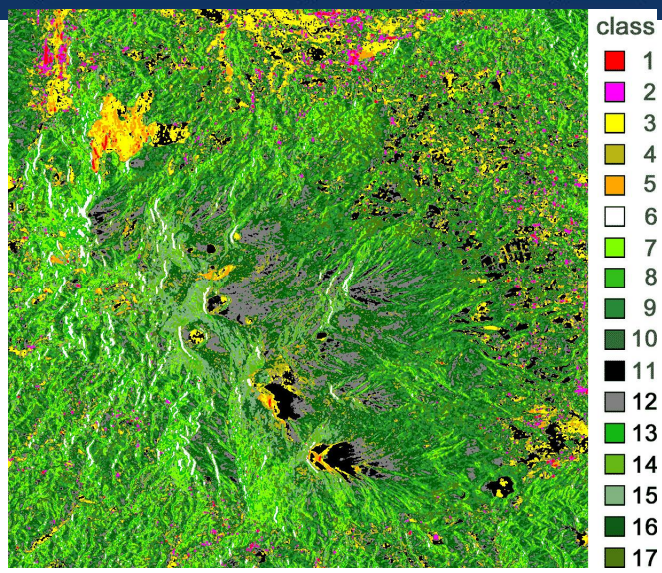

Figure 8: The classified result of 17 classes of the image after the eruption.

The image after the eruption on 16 March 2011 was classified by the same way. Figure 7 shows an image of the total power component of the original image. Although the figure of the concordance rate *C* versus the class number *N* is not shown, the optimum class number *Nc* is 17, and that the *Nc* is 6 classes more than the number of the image before the eruptions. Figure 8 is the classified result of the optimum total class number 17.

INTERPRETATION OF CLASSIFIED RESULTS BY THE FOUR-COMPONENT SCATTERING MODEL

Each class of the classified results of the images before and after the eruption is interpreted by using the four-component scattering model (Yamaguchi, 2005). Figure 9 and Figure 11 show the normalized total powers obtained by dividing total powers of each class by the maximum total power. Figure 10 and Figure 12 show the ratio of four components on the total power of each class. Figure 9 and Figure 10 are for the image before the eruption and Figure 11 and Figure 12 are for the image after the eruption. Comparing Figure 9 and Figure 10 with Figure 11 and Figure 12, the polarimetric characteristics from the class 1 to the class 11 of each image are similar and correspond respectively.

To begin with, characteristics of these 11 classes are interpreted with Figure 9 and Figures 10. Class 1 has the largest value of total power *Tp*. Eighty percent of the *Tp* is occupied by surface scattering power P_s. This class represents targets whose backscatter Radar Cross Section (RCS) is extremely large and these targets spread across urban areas. Class 2 has the fourth largest *Tp*, and the ratio of double-bounce scattering power P_d is larger than other classes. This class represents an urban area composed by buildings with vertical wall surfaces. Class 3 has small *Tp*. Sixty percent of the *Tp* is occupied by the P_s, and represents a bare area and a grass field. Class 4 has little smaller Tp. The deviation of the four power components is small. Trees, grass land and buildings coexist in the area of this class. Class 5 has the third largest *Tp*. Eighty one percent of the *Tp* is occupied by the P_s. This class represents targets whose surface faces to the satellite or where reflection of an odd number of times occurs. Those targets appear throughout and around urban areas.

Class 6 has the second largest *Tp* and represents the area of layover in a mountainous area. Class 7, 8, 9 and 10 represent forests. The composition ratio of Class 7 is different from the other three classes. Class 7 appears on a cismontane slope looking from the satellite. On the cismontane slope, the smaller incident angle than the three classes results on the larger ratio of P_s and the larger value of *Tp*. On Class 8, 9 and 10, the largest ratio of the P_v (about 45 percent) express that these classes are forests, and the composition ratios of the four-components are almost identical. Class 8, 9 and 10 appear on a flat area, a lower part of the tramontane slope and a higher and steeper part of the tramontane slope, respectively. Because incident angles of these classes increase in turn from class 8 to class 10, values of *Tp* decrease in the same order. Class 11 has the lowest value of *Tp*. This class represents a water surface, a paddy field and the shade portion of the RADAR wave on the tramontane steep slope and inside of the crater.

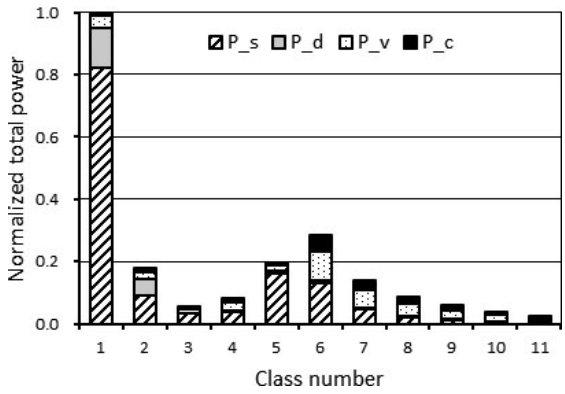

Figure 9: Normalized total power of the 11 classes of the image before the eruption. P_s: surface scattering, P_d: double bound scattering, P_v: volumetric scattering, P_c: helix scattering.

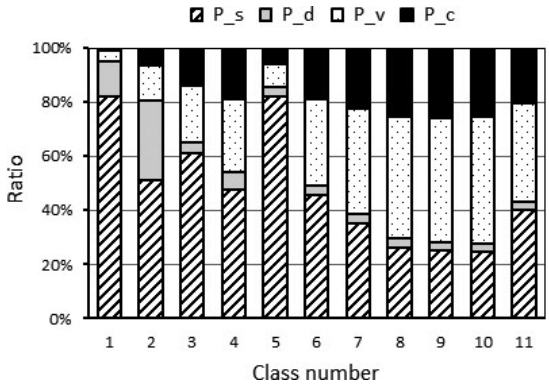

Figure 10: The ratio of the four components of the classes of the image before the eruption.

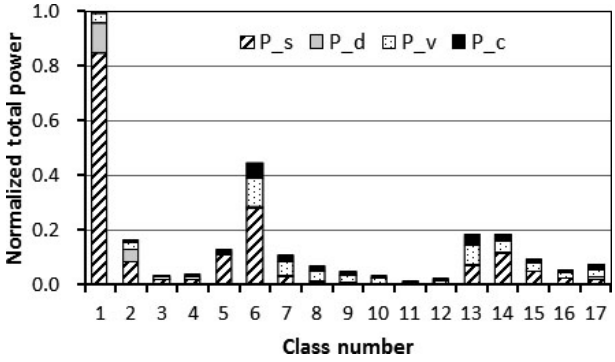

Figure 11: Normalized total power of the 17 classes of the image after the eruption.

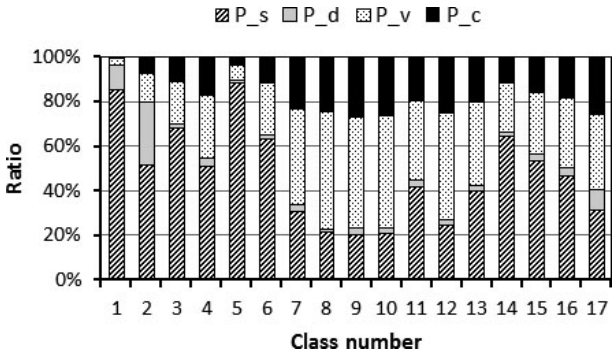

Figure 12: The ratio of the four components of the classes of the image after the eruption.

Next, characteristics of the remaining six classes, which appear newly in the image after the eruption, are interpreted. The composition ratio of the power components of Class 12 is almost same as the ratio of Class 8, 9 and 10. However, the value of *Tp* is half smaller than those classes. Class 12 appears on the tramontane steep slopes close to the summits of Shinmoedake and adjoining volcanos. Because an incidence angle is large on these tramontane slopes, reduction of surface roughness by deposition of the eruptions decreases back-scattering. This is the reason why the value of *Tp* becomes smaller.

Class 13 appears on the cismontane slopes and it has larger ratio of P_s and larger values of *Tp* than Class 7. It seems that these were caused by reduction of surface roughness by the deposition on the area of Class 7. Class 14 appears on the area just under the layover where an incident angle is small and deposition is deeper. In the upper portion of class 7, ratio of P_s was increased until the composition ratio was similar to Class 6 by the reduction of the surface roughness and resulted on the larger value of *Tp* than Class 7.

Class 15 appears on the slope under the border of Class 14. It seems that the composition ratio of Class 15 was shifted on the same way as Class 14.

Class 16 appears on some areas of Class 9. Although the increase of Tp was little, the ratio of P_t was much increased. The reason why these were caused is not clear. Class 17 has the larger ratio of the double bound scattering than other 5 classes which appeared newly in the image after the eruption. Class 17 appears in the forest of the lower part of slopes and the plain. Because trees grow almost vertical on these gentle slopes and in the plain, there is the double bound scattering caused by the reflection between ground surfaces and trunks. Furthermore reduction of surface roughness by deposition of volcanic products increases the surface scattering and resulting the double bound scattering.

CONCLUSIONS

POLSAR images of ALOS PALSAR of Shinmoedake volcano in Kyushu, Japan were analyzed. Eruptions of the volcano on 26th and 27th January, 2011 caused ash depth of more than 10 cm in 12 km^2 and 1 m in 2 km^2. Two images before and after the eruption were classified by the unsupervised classifier with the Wishart distance The optimum total number for the classfier is fixed by inspecting results with which two sets of different initial clusters converged. Varying the total number N of the classes of each set simultaneously, the optimum number Nc is set as the N which makes the concordance ratio of the converged results minimum. The optimum total numbers of classified categories of the two images of the volcano are 11 and 17, respectively. From a view point of the four-component scattering model, the 11 categories can be coupled with the similar categories of the image after the eruption. Because remaining 6 categories changed the normalized total power and the ratio of surface scattering power to the total power, they are different from the 11 categories. Moreover, the ratio of double-bounce scattering power increases in one of the 6 categories

ACKNOWLEGEMENTS

This research was accomplished by the activity of the Group of Analysis of Satellite Data, the Coordinating Committee for Volcanic Eruption Prediction, Japan and by the found of MEXT-Supported Program for the Strategic Research Foundation at Private Universities..

REFERENCES

Cao, F., Hong, W., Wu, Y. and Pottier, E., 2007. An unsupervised segmentation with an adaptive number of clusters using the SPAN/H/α/A space and the complex Wishart clustering for fully polarimetric SAR data analysis. IEEE Trans. GRS, 45(11), pp.3454-3467.

Lee, J., Grunes, M., Ainsworth, T., Du, L. and Schuler, D., 1999. Unsupervised classification using polarimetric decomposition and the complex Wishart classifier. IEEE Trans. GRS, 37(5), pp.2249-2258.

Japan Metrological Agency (JMA), 2011, Transactions of the 120th meeting of the Coordinating Committee for the Prediction of Volcanic Eruption (in Japanese), pp.35.

Lee, J., Grunes, M., Pottier, E. and Famil, L., 2004. Unsupervised terrain classification preserving polarimetric scattering characteristics. IEEE Trans. GRS, 42(4), pp.722-731.

Ohkura, H., Ukawa, M., Yamaguchi, Y., 2011, An optimum total number of classes of the unsupervised Wishart classifier for fully polarimetric SAR image data, ACRS2012, CD-ROM.

Yamaguchi, Y., Moriyama, T., Ishido, M. and Yamada, H. 2005. Four-component scattering model for polarimetric SAR image decomposition. IEEE Trans. GRS, 43(8), pp.1699-1706.

Xu, F. and Jin, Y., 2005. Deorientation theory of polarimetric scattering targets and application to terrain surface classification. IEEE Trans. GRS, 43(10), pp.2351-2364.